Drying of a colloidal suspension in confined geometry

Jacques Leng*
Laboratory of the Future, Université Bordeaux-1, 178 Avenue du Docteur Schweitzer, 33608 Pessac Cedex, France
(Received 6 May 2010; revised manuscript received 20 July 2010; published 23 August 2010)

We describe experiments on drying of a hard-sphere colloidal suspension in confined geometry where a drop of the suspension is squeezed in between two circular transparent plates and allowed to dry. In this situation, the geometry controls the vapor removal rate and leads to a facilitated observation directly inside the drop. We monitor the drying kinetics of colloids of two sizes and several volume fractions; in most cases, the drying kinetics leads to the formation of a crust at the level of the meniscus which can be either crystalline or glassy, the transition between the two cases being triggered by the local deposition velocity, itself slaved to the evaporation rate. It yields a final dry state which is either polycrystalline or amorphous. The crust is also responsible for a shape instability of the quasi-two-dimensional drop shrinking upon evaporation but with a crust opposing mechanical and flow resistance, and possibly a partial adhesion on the substrate.

DOI: 10.1103/PhysRevE.82.021405 PACS number(s): 82.70.Dd, 47.57.ef, 81.16.Dn

I. INTRODUCTION

Drying is a fascinating and ubiquitous phenomenon: it selects natural geometries and morphologies, has an important role in the technology of coating processes, and is an obvious and major step in the industrial production of a large gamut of end products, from foodstuff to civil engineering materials.

While the conditions in which drying occurs may vary drastically depending on the process, the basic case of the sessile droplet of a solution evaporating in air at room temperature has attracted a tremendous academic interest, and delivered valuable information. It represents a simple experimental situation which catches the complexity of drying: surface tension, line pinning, and vapor removal are coupled to induce a capillary flow which controls the deposit during drying [1–3], whereas Marangoni effects also play a crucial role [4–7]. Even if a theory that fully describes these systems remains challenge and complex [8–13], these evaporation-induced flows have opened up creative routes to shape-up new and original nano- and micromaterials [14–17].

Recent experimental breakthroughs were obtained on model systems or via sophisticated observation. Two-dimensional surface drying [18,19] for instance includes theory, simulation, and experiments and permits to understand thoroughly the interplay between thermodynamics and kinetics in the final state. Yet, bulk drying is clearly more difficult to investigate essentially because of observation limitations and much has been inferred on the basis of global observations [20–22]. The recent development of noninvasive, fast, and local measurements, such as confocal spectroscopy and microscopy, will permit to image optically or chemically the bulk of a sample [23–28]. This, together with the use of controllable soft matter systems, might help revisit and unveil the physics at work in bulk drying, and especially to appreciate how rheology, kinetics, and thermodynamics are also coupled to the capillary flows.

In this work, we present a simplified version of the drying experiment which permits to bypass some of the experimental difficulties of bulk drying. It consists in confining a drop of a solution in between two plates as described in Fig. 1, and has two strong consequences on the drying process: first, the kinetics is imparted by the geometry as boundary conditions for evaporation are not left at infinity but instead are set by the geometrical extent of the plates [29]; then observation is made easy due to the thin, quasi-two-dimensional (2D) geometry. This contrasts with the case of a sessile droplet which is intrinsically a three-dimensional (3D) problem.

Based on the experimental observation and qualitative arguments, we demonstrate that such a 2D geometry is quite fruitful to revisit most of the well-known results concerning the drying, here of a model hard-sphere (HS) colloid suspension: evaporation induces the buildup of a dense state, a crust, at the edge of the drop which inhibits the volume decrease and induces a buckling instability of the drop (like the invagination of a solid shell [20,21]). The crust, which can be ordered or amorphous, grows quickly and totally invades the drying drop; eventually, it dries up completely and frac-

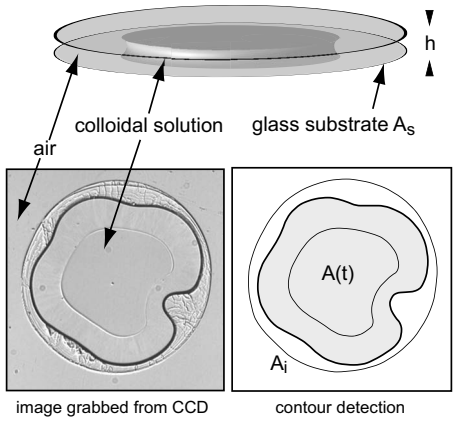

FIG. 1. Schematic view of the confined drying geometry where a droplet of a colloidal solution ($\approx \mu$L) is squeezed in between two circular glass plates (diameter $\approx$8 cm) and let to dry up. A camera captures the image (here of size 4 mm) and is further processed for contour detection.

*Previous Address: School of Physics and Astronomy, the University of Edinburgh, Edinburgh EH9 3JZ, United Kingdom; jacques.leng-exterieur@eu.rhodia.com

tures. We eventually demonstrate with simple arguments that the drying kinetics can be entirely understood at least qualitatively on the basis of the confinement and local dynamics of the colloids, and that the present experiment indeed delivers an extra optical observation of the kinetics *seen from inside the drop* which is not directly accessible in 3D drying experiments.

II. MATERIAL AND METHODS

A. Colloidal suspension

The colloidal solution we used was synthesized and kindly provided by Dr. Andrew B. Schofield (http://www.ph.ed.ac.uk/~abs/). It consists of poly-(methyl methacrylate) (PMMA) spheres coated with a thin (≈ 10 nm) poly-(12-hydroxystearic acid) layer and dispersed in *cis*-decalin, a model system for HS colloids [30,31]. We used two sets of solutions differing by the radius of particles, namely $R_p=(230\pm 10)$ nm and (3 ± 0.1) μm hereafter termed *small* and *large* colloids respectively. For the small specie, the volume fraction may vary between $\phi_i=0.2$ and ≈ 0.6, while for the large one the maximum volume fraction is about 0.3.

The solvent, *cis*-decalin, has a very small vapor pressure which sets a slow evaporation kinetics ($p^\star \approx 120$ Pa at 20 °C [29]; compare to water $p_w^\star \approx 2.4$ kPa). Besides, there is hopefully no decalin vapor in air which permits to disregard the issues related to the relative "humidity." At room temperature, the density of this liquid is $\rho \approx 900$ kg m^{-3}, its viscosity $\eta \approx 3$ 10^{-3} Pa s, its surface tension with air is $\gamma \approx 31$ 10^{-3} N m^{-1} [32] which varies with temperature like $\partial_T \gamma \approx -0.1$ 10^{-3} N(m K)$^{-1}$ (see http://www.surface-tension.de/).

B. Confined drying

When a drop of a pure solvent is squeezed in between two plates, just like in Fig. 1, we may assume that evaporation proceeds by diffusion of the gas from the meniscus of the drop, where the atmosphere is assumed to be saturated in vapor, toward the edge of the cell where the atmosphere is dry. If the height of the cell is small as compared to its lateral extent, the geometry is quasi-2D and the rate at which a drop shrinks is calculated by flux conservation at the level of the meniscus and near-equilibrium assumption: the vapor that diffuses away from the interface just contributes to diminish the volume of the drop [29]. It follows that *for a pure liquid*,

$$\ln \alpha \frac{\mathrm{d}\alpha}{\mathrm{d}t} = \frac{1}{\tau_e}, \tag{1}$$

in which $\alpha(t)=A(t)/A_s$ is the area of the droplet $A(t)$ normalized by the area of the substrate A_s, and $\tau_e=A_s/4\pi\tilde{D}$ the evaporation time; $\tilde{D}$ represents the diffusion coefficient of the gas modified to account for density balance between the liquid and the gas. This result shows that confining the evaporation casts a specific kinetics to the evaporation process, which is due to the finite size of the substrate from which the gas must escape, and can therefore be tuned fairly easily by changing the size A_s of the substrate.

Here, we used a glass substrate with a radius $R_s=4$ cm and a thickness 1 mm, and no surface treatment but thorough cleansing with detergent. Three linear spacers of plastic shim (thickness $h=50$ μm) were used in all experiments and ensure a quasi-2D cylindrical geometry. We obtain experimentally that $\tilde{D}=(4.2\pm 0.03)10^{-11}$ m^2 s^{-1} at $T=23$ °C for pure decalin [29].

C. Observation and analysis

We use both local and global optical monitoring, although not simultaneously, to observe the drying kinetics. The large scale view is based on a simple optical rig which combines a couple of lenses that permit to observe the entire drop, of typical radius of the order of a millimeter, with a resolution on size measurement of order of 50 μm [29]. The images are acquired with a charge coupled device camera and frame-grabbed on a computer, and are then mathematically processed in order to extract the instantaneous features such as area $A(t)$, perimeter $P(t)$, connectivity, etc. The time resolution we used is sufficient—typically 1 Hz for a kinetics that spans a few hours—to obtain a fine description of the drying.

We also used standard bright field, phase contrast, and polarized microscopy to observe locally the formation of the solid deposit and the formation of a crust that both occur during the course of drying.

III. RESULTS

A. Time series: shrinking, drying, and fractures

We display in Fig. 2 two series of snapshots of the temporal evolution of the colloidal droplet undergoing drying for small and large colloids confined in the same cell. In both cases, the experiment begins with a nearly perfectly circular droplet which starts receding as a consequence of the controlled vapor removal. Soon after, a front *inside the drop* becomes visible. With time, the size of the drops keeps diminishing while the inner front moves inward. The drops does not keep a perfectly circular shape but instead, an instability develops which produces an invagination, except at the highest initial volume fractions ($\phi_i \gtrsim 0.55$) where the drop always remains circular [33].

Once the inner front has merged centrally, the 2D drop reaches its final state, whose geometry depends drastically on the initial volume fraction and on the size of colloids; there is then a latency time during which the area remains constant [$A(t)$ plateau in Fig. 3, top], and the ultimate stage of the process consists of cracks and fractures propagation, and the drop becomes eventually totally opaque. Such a massive darkening is due to the raise of the refractive index difference between the particles (PMMA, $n \approx 1.49$) and the interstitial fluid made first of decalin first ($n \approx 1.47$) and then replaced with air ($n \approx 1$) upon drying.

The whole process is actually better seen in a video supplied as a supplementary material [34]. While out of the scope of the present work, we also clearly see that the hierarchical skeleton of the fractures along with the ultimate dry-

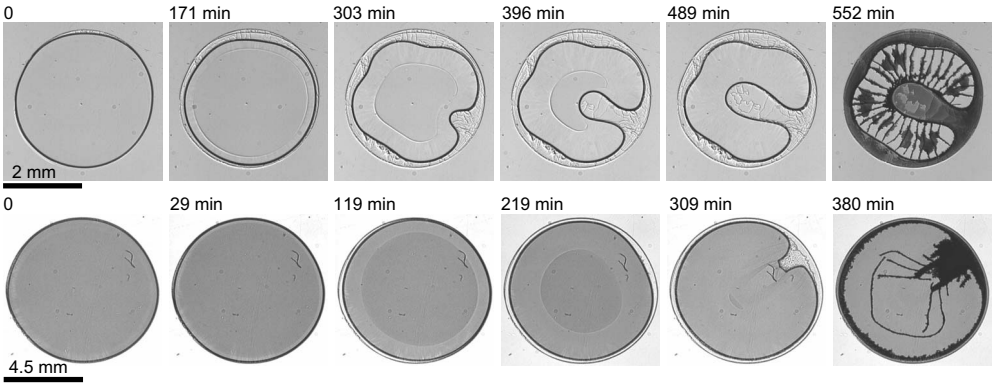

FIG. 2. Series of pictures showing the confined drying of a drop of a colloidal solution of PMMA particles in decalin (top: small colloids with a particle radius R_p=230 nm at an initial volume fraction ϕ_i=0.44; bottom: large colloids with R_p=3 μm, ϕ_i=0.1).

ing process strongly depend on the size of the colloids (see for instance the last picture of the two series in Fig. 2): for the small ones, the cracks propagate radially while pockets of dry matter nucleate inside what remains of the solution, and further grow until the whole drop has dried up; for large colloids instead, a crack follows a looped pattern while the drying front nucleates at the edge of the drop and propagates inwardly. Interestingly, for small colloids the fracture skeleton also follows this type of looped pattern but only for concentrated enough solutions ($\phi_i \gtrsim 0.55$, not shown).

Automated measurements using image analysis permit to quantify this behavior; we actually focus on the time evolution $A(t)$. In *all* the cases we monitored, the area decreases *linearly* with time until it reaches a plateau (Fig. 3, top), while the perimeter also decreases linearly for a while before shooting up as a sign a the shape instability [35]. The first and most straightforward measurement we obtain from the image analysis is the ratio A_f/A_i of areas at the end A_f and at the beginning A_i of the experiment. A_f corresponds to the plateau in $A(t)$ at the late stage of drying, just before the drop effectively dries up and fractures (see for instance Fig. 2, A_i at t=0, and A_f at t=489 min). This ratio is a function of initial volume fraction of the colloidal suspension and we found that:

(i) for small colloids, there is linear relationship between A_f/A_i in the range ϕ=0.2–0.55 (with a slope 0.74 ± 0.03) and then a deviation to linearity above $\phi_i \approx 0.55$ (Fig. 3, bottom);

(ii) for large colloids, the ratio depends on initial conditions, is always smaller than 0.65, and behaves in a less systematic way (data not shown).

B. Crust effect

One of the striking effects depicted here and common to many of the drying patterns is the formation of a *crust*, namely, a front which separates two regions and whose border is shifting toward the center of the drop with time, Fig. 2.

Local observation with optical microscopy reveals that the crust has a structure which depends significantly on the colloidal solution. Figure 4 shows a detailed set of micrographs collected at several locations (shown in the inserts) in and out the drying drop. For small colloids [Figs. 4(a)–4(c)], the crust is quite organized. Figures 4(a) and 4(b) show two identical views but with a different contrast; the pictures display a directional structure of needlelike shapes of a few hundreds of micrometers of width and several millimeters long. The long direction of the needlelike objects is parallel to the growth direction of the crust, which strongly suggests that texture is induced by the growth process.

In between crossed polarizers, the objects appear weakly birefringent, and the linear shape of the texture is also confirmed. Such a strongly anisotropic structure is very reminiscent—if not identical—to the ones observed during settling of a colloidal suspension [36] which indeed produces long columnar crystals [37]. By contrast, for the large colloids optical microscopy reveals no structure.

During the drying, the drops leave behind a thin deposit. We focus here on the top series of Fig. 2, e.g., image two (at

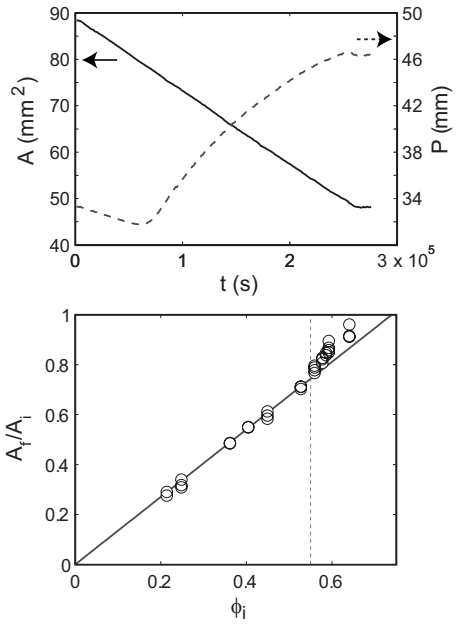

FIG. 3. Top: measurements of area A and perimeter P against time t obtained from the image analysis (here for small colloids at ϕ_i=0.4). Bottom: ratio of area at the end of the drying kinetics A_f to the initial area A_i against the initial volume fraction ϕ_i. The straight continuous line has a slope 0.74. The vertical dashed line is positioned at ϕ_i=0.55.

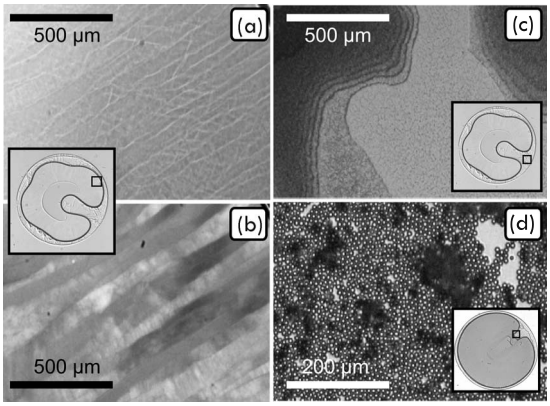

FIG. 4. Micrographs of the crust with different optical contrasts [(a) phase contrast and (b) crossed polarizers] in the case of small colloids at relatively high volume fraction (ϕ=0.44); optical micrographs of the deposit leftover outside the drying drop for small colloids (c) and large colloids (d). In all cases, the insert shows where the pictures were taken.

t=171 min), for which there are several levels of contrast: the most marked (dark) ring corresponds to the vapor/liquid meniscus. Just outside of it, there are marks lefts behind the meniscus after its recession; this is an actual case of convective deposition [38,39] of a liquid moving on a substrate in wetting conditions. Bright field microscopy imaging reveals two scenarios depending on the size of colloids. For small colloids, one observes spectacular terraces [Fig. 4(c)], whereas for larger beads, the system is totally disorganized [Fig. 4(d)] with a local amorphous structure and plenty of voids. We will see later on how this impacts the drying kinetics.

Local and global imaging where used to record the velocity at which the crust grows and we focus here only on the case of small colloids. The growth behavior (front position x_c measured from the edge of the drop) is initially linear with time then speeds up although this behavior is sometimes not so clear. We define the growth velocity of the crust v_c as the initial slope of $x_c(t)$ and show in Fig. 5(a) that by changing the size of the drop R_0 while keeping ϕ_i constant, the crust velocity scales like $v_c \sim -[R_0 \ln(R_0/R_s)]^{-1}$, which is actually proportional to the diffusion-limited evaporation rate of the solvent that escape from the drop (see Ref. [29] and also Sec. III). Then, by tuning the concentration in the drop while keeping its size constant, we observe a strong dependency of $v_c \sim \phi_i/(0.74-\phi_i)$ with the content of the drop which, as we shall see latter on, is well described in terms of conservation laws and truncated dynamics.

IV. DISCUSSION

In Sec. II B, we recalled how the confined geometry casts a control on the drying process essentially because the solvent vapor escapes the cell by a diffusion-limited kinetics between the meniscus of the drop and the edge of the cell, in a first approximation; the corresponding time scale directly depends on the size of the substrate [29] and reads $\tau_e = R_s^2/4\tilde{D}$ where $\tilde{D}$ is a modified diffusion coefficient of the

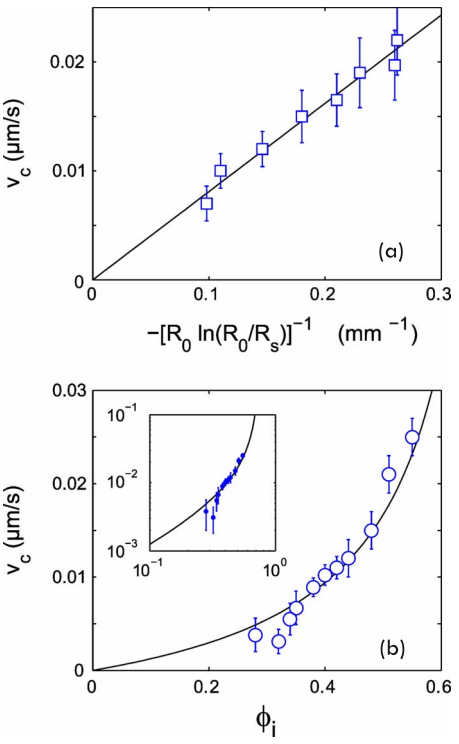

FIG. 5. (Color online) Growth velocity of the crust as a function of (a) a reduced evaporation flux expressed here with the size of the drop radius R_0 (mm) and substrate radius R_s (see text; for ϕ_i =0.44, small colloids) and (b) as a function of the initial volume fraction ϕ_i at constant drop radius R_0 constant (insert: same data in log scale). In (b), the solid line is a fit based on conservation laws [Eq. (3) and corresponding text] $v_c = A\phi_i/(0.74-\phi_i)$ with A =$(8\pm1)10^{-3}$ μm s^{-1}.

gas in air. When loading the solvent with a solute, here a colloidal dispersion, a number of thermodynamic and kinetic effects add up a significant complexity to the evaporation process. The main thermodynamic effect, which we directly elude, consists in principle of the modification of the chemical potential of the solution as a function of the composition. According to Raoult's law, we expect a decrease in the pressure of the vapor in equilibrium with the solution, which will in turn slow down evaporation; however effect is negligible in the case of large objects such as 200 nm colloids, while it remains relevant for solutions of small molecules [29].

Other effects are well delineated with the use of dimensionless numbers which compare several transport properties in the fluid. The natural and typical time scale is that of evaporation τ_e ($\approx 2\times10^6$ s for decalin confined in a substrate of radius R_s=4 cm) while the spatial scales are given by R_s and h, the radius and the height of drying cell respectively. A typical velocity thus scales like $v \sim R_s/\tau_e$ =$\mathcal{O}(10^{-2}$ μm s$^{-1})$ [40].

The Reynolds number calculated on the height of the cell with the properties of decalin is extremely small (Re $<10^{-4}$) and any flow shall be laminar and well described by the lubrication approximation.

The Péclet number (Pe$\equiv v_m R/D_p$) which compares the diffusion of colloids (with a diffusion coefficient $D_p \approx 3.1 \times 10^{-13}$ m^2 s^{-1} calculated using the Stoke-Einstein relation)

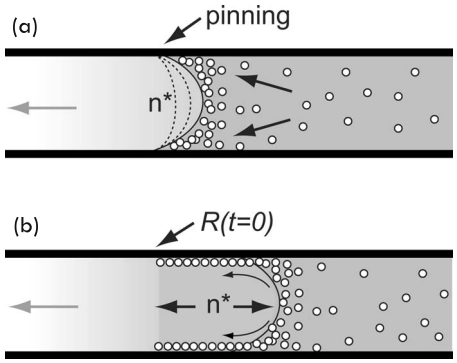

FIG. 6. Schematic illustrations of the mechanisms at work at the level of the meniscus. In (a), the pinning of the contact line prevents the meniscus to recede, which induces a compensation flow and ultimately drives the colloids toward the meniscus. If the latter nevertheless recedes, it leaves behind a deposit of colloids [(b) see also Fig. 4(c)] which sustains an atmosphere at the saturation concentration $n^\star$.

along the radius R of the drop to the convection induced by the evaporation is large ($\approx 10^2$). Therefore, Brownian motion will never be able to balance concentration gradients potentially produced by convection. Put another way, the typical size onto which concentration gradients develop D_p/v_m is very small (≈ 0.1 μm).

Due to evaporation, thermal gradients may develop and induce a flow [4,5,7]; confinement however is likely to prevent it. The Marangoni number compares the surface-induced stress to the dissipation forces, and reads: $\mathrm{Ma} \equiv (-\partial\gamma/\partial T)h\Delta T/(\eta\alpha)$ where α is the thermal diffusivity ($\approx 10^{-5}$ m^2 s^{-1}). Therefore, evaporation for confined decalin producing a typical temperature shift of $\Delta T \approx 0.01$ K leads to $\mathrm{Ma} \approx 10^{-3}$. No significant recirculation flow is expected from thermal-induced gradients.

This contrasts with capillary flows induced by surface deformation. Indeed, as the capillary number $\mathrm{Ca} \equiv \eta v_m/\gamma \approx 10^{-9}$ is very small in our case, the surface tension is likely to dominate any surface deformation, often linked to line pinning. Whenever this occurs, a capillary flow will compensate the mass imbalance as compared to a freely moving meniscus. This is schematically depicted in Fig. 6(a).

This survey gives a flavor of the process: vapor removal is controlled by the confinement, which provokes the displacement of the wetting meniscus. In the frame of the moving meniscus, the colloids are getting accumulated close to the meniscus which will explain of the occurrence of the crust. Such an accumulation is likely to be enhanced by capillary flows but not thermal recirculations. We now examine this scenario in details.

A. Drying at constant rate

We actually observe in all the experiments that the time evolution of the area is constant: $\dot{A} = \text{const.}$ (Fig. 3), seemingly in contradiction with the evaporation Eq. (1); the latter rather predicts a logarithmic correction coming from the cylindrical geometry but holds only for pure liquids, not dispersions.

We suggest that this constant kinetics is due to the convectively deposited material left behind the meniscus. Indeed, as suggested in Fig. 6(b), when the meniscus recedes and leaves a colloidal film behind, the atmosphere in between the upper and lower films is likely to remain saturated with vapor; an alternative way to put it is to assume that the evaporation occurs only *at the rim of the film*, around the singularity at $R(t=0)$ in Fig. 6(b). It is also clear from an experimental point of view that this region becomes effectively dry only at the final stage of the kinetics, see for instance the last image in Fig. 2, at $t=552$ min, where the film left behind becomes dark.

The evaporation condition is thus set by the initial size of the drop A_0 and by drainage across the film formed via capillary/convective deposition. Therefore, we may assume there is a *constant* flux of solvent escaping from the initial trace of the drop at a radius $R(t=0)=R_0$ that reads [29]:

$$J_0 = -\frac{\rho_L \tilde{D}}{R_0 \ln(R_0/R_s)}, \tag{2}$$

in mass per unit of time and area, where ρ_L is the mass density of the liquid decalin. Such a constant evaporation flux is directly responsible for a constant mass loss, or equivalently in our 2D geometry a constant surface loss, as indeed observed experimentally.

B. Truncated dynamics and capillary flow

The combination of a constant mass loss and large Péclet number has a direct consequence *on the accumulation of the colloids* around the meniscus. Indeed, in the frame of the meniscus, there is a flow of liquid that brings more and more colloids which therefore tend to accumulate (even if a small quantity is left behind by convective deposition). The concentration profile in the fluid phase is expected to resemble that of sedimentation, close to an exponential with a typical size D_p/v_m; as this "sedimentation length" is small ($D_p/v_m \lesssim 0.1$ $\mu\mathrm{m} \ll h$), it is hardly noticeable experimentally and the sample remains essentially homogeneous. The magnitude of the concentration gradient increases linearly with time at the level of the meniscus, at least initially [41], and will in any case reach ultimately a concentrated regime. This is the occurrence of the crust with a solid/liquid border, a shock front, which has been observed either in 3D [20,21] or directional drying [42,43], and recently referred to *a truncated dynamics* [8,12,13].

Zheng [13] derived the dynamics of such a front based on conservation laws in an axial flow. If we develop his result around $t=0$ in the frame of the moving meniscus at a velocity $v_m = -J_0/\rho_L$ derived from the fixed evaporation rate [Eq. (2)], and a homogeneous concentration field at $\phi=\phi_i$, the growth rate of the crust v_c follows:

$$v_c = v_m \frac{\phi_i}{\phi_{\max} - \phi_i}, \tag{3}$$

where $\phi_{\max}$ is the concentration at truncation.

While we have good agreement for the scaling of $v_c \propto v_m$ at a given volume fraction [Fig. 5(a)], which indeed

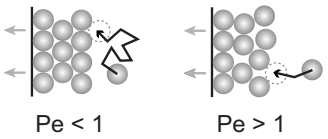

FIG. 7. A schematic view on the impact of the local Péclet number on the growth process. (Left, $\mathrm{Pe}<1$) Diffusion dominates and the spheres can explore many conformations before finding a registered crystalline position; the structure will be organized. (Right, $\mathrm{Pe}>1$) Convection dominates and does leave any chance to the colloids to reach a registered position; the structure is likely to be disordered.

supports a direct coupling between the solvent removal rate and the crust growth, we also recover a satisfactory scaling—see Fig. 5(b)—assuming (i) v_m is fixed and (ii) $\phi_{\max}$ is constant. The former point is reasonable as the crust velocity is measured at its early stage of appearance, when the size of the drop has not changed too much; it is also consistent with the observation of constant solvent removal rate, Eq. (2) With these assumptions, we obtain that the fit procedure gives $v_m \approx (6 \pm 1) \times 10^{-9}$ m s^{-1} in good agreement with the direct calculation $v_m = -J_0/\rho_L$ which yields $v_m \approx 8 \times 10^{-9}$ m s^{-1}. Here, we kept $\phi_{\max}$ constant and fixed at the maximum compacity value (i.e., that of a compact crystal $\phi_{\max}=0.74$), consistently with the observation of the crust structure that we will give now.

C. Structure of the crust

The process of the crust formation leads to a deposit which is organized or disordered depending on the conditions of volume fraction and particle size. The crust seen in Figs. 4(a) and 4(b) obtained at moderate volume fraction of small colloids resembles very much the columnar structure obtained during the settling of the same colloids, in which case the iridescent aspect proves the crystalline nature.

Here, on top of the apparent birefringence [Fig. 4(c)], the measurement of the volume fraction is another type of proof: if we disregard the colloids lost on the substrate by convective deposition, we can assume that the volume of colloids is conserved, thus $A_i\phi_i = A_f\phi_f$. It results that the area measurement provides a simple way to estimate the concentration at the end of the drying process (Fig. 3). For most cases of small particles, we observe that the volume fraction at the end of drying is $\phi_f \approx 0.74$, i.e., that of a close-packed systems. This is however untrue (i) for systems of small particles when starting at high concentration, namely, $\phi_i \gtrsim 0.55$ where the final volume fraction is smaller than 0.74 and (ii) for systems of large particles.

This behavior is usually explained with the help of the Péclet *defined locally* on the size of the particle $\mathrm{Pe} = vR_p/D_p = 6\pi\eta R_p^2 v/kT$. If using the value of the crust velocity measured in Fig. 5(a) and the viscosity of pure decalin, we find that $\mathrm{Pe} \approx 0.1 \ll 1$ for small particles, but $\mathrm{Pe} \gtrsim 1$ for large particles. The Fig. 7 illustrates schematically the possible interpretation: for a small Péclet number, the diffusion dominates close to the crust and the particles will explore several configurations before smoothly finding a registered position that is on a crystalline site; it is obviously guided by the flow field in the interstice of the lattice. Oppositely, when the Péclet number is large, the particles get trapped and locked in any position of a more open, glassylike structure. The transition between the two limits is triggered by a shift in particle size and also in concentration as the viscosity increases strongly when the concentration raises.

We observe experimentally the two behaviors either by increasing significantly the size of the colloids or by increasing the viscosity of the solution of small colloids. Indeed, for $\phi_i \gtrsim 0.55$, the system is prepared in a metastable liquid state, which shall crystallize but does not for kinetic reasons; it thus reaches quickly a glassy state upon evaporation, which is viscous and does not leave the small colloids any chance to reorganize locally to find a registered position. It eventually leads to a final deposit with a low compacity ($\phi_f < 0.74$).

D. Buckling of a 2D shell

Once the deposit starts to grow, it has a tremendous effect on the rest of the drying kinetics; it will in some cases result in the invagination process that we observe in Fig. 2. Our observations actually closely follow 3D experiments concerning the buckling of shells obtained by evaporation of drops with colloids [20–22,44]. The onset of the buckling instability is due to the mechanical resistance that opposes the crust upon the constraint of evaporation that forces the volume to shrink: the crust can either flow, get compressed or buckle depending on its mechanical and geometrical features. The crust also has a significant impact on evaporation, either via the capillary pressure that may diminish the vapor pressure, especially for very small colloids, or because of the viscous dissipation in the porous medium that makes up the shell [20,42,43].

It is interesting to see that we recover the exact sequence of reference [20] with only one obvious difference, beside our 2D geometry: several modes of deformation occur before one wins over the others; the latter will develop largely and produces an invagination. It is due to the fact that once deformed, a concave meniscus is likely to become saturated with vapor and will then be less prone to evaporation. The local driving force for the crust formation hence fades away and the crust becomes inhomogeneous. When looking closely, it is even possible to observe that the crust redissolves (or melts away) at the level of the invagination, as for instance in Fig. 2 at $t=396$ min.

Beside, there is also an interaction of the crust with the substrate which is present at 2D and not at 3D. Indeed, in case of any interaction of the colloids with the substrate, e.g., van der Waals attraction, an additional resistance is created and prevents the crust to recede further. This hypothesis has been checked experimentally recently [45] by tuning the nature of the substrate: it turns out that the onset of the instability indeed depends specifically on the substrate and is delayed in case of a lubricating substrate, which accredits the role surface anchoring to induce an invagination instability. The exact way the colloid/substrate interaction plays a role has not been detailed but should be workable in principle due

to the neat control of geometry and observation.

V. CONCLUSION

The present work focuses on a qualitative picture of the drying of a colloidal solution in a confined geometry, with some variations as to the degree of confinement. The observations span some of the typical events that occur during drying that are, most of the time, observed in 3D and sometimes in directional drying. The quantitative scenario depicted here seems quite clear, thanks to the facilitated 2D observation: due to evaporation, colloids get accumulated at the edge of the drop where they will eventually prevent an homogeneous recession of the meniscus; it produces a shape instability which is related, in principle, to the mechanical stiffness of the crust and flow properties across such a porous crust, and possibly to the substrate/colloid interaction. The local dynamics characterized by the local Péclet number can then select the structure of the crust, either crystalline or amorphous, which in turn also selects the structure of the final dry state.

The possible strength of the simple drying strategy presented here lies in the ready-to-use geometry and the good control it yields for quantitative studies. The next steps of investigation will consists on the one hand in calculating numerically the concentration field inside the drop (equation are writable but not tractable analytically [41]), and on the other hand in measuring these concentration fields inside the drop, against space and time, as for instance with Raman spectroscopy [46] or fluorescence techniques to extract velocity and mobility fields (with tracer velocimetry and microrheology [28]) along with the concentration fields [23,24]. It could give, in principle, a facile route to investigate the more complex case of bulk, 3D drying.

ACKNOWLEDGMENTS

We thank F. Clément for permanent enthusiasm, M. E. Cates, S. U. Egelhaaf, W. C. K. Poon, and J.-B. Salmon for discussions and support, and A. B. Schofield for providing the state-of-the-art HS colloids.

APPENDIX: ADDITIONAL EXPERIMENT ON CONFINED DRYING

We anticipated that capillary effects must be dominant at a very small Ca and we exemplify it now with a complementary experiment showing that the buildup of the crust does proceed through a strong role of the pinned interface. This is just another drying experiment *in confined geometry* where a drop of the colloidal solution is even further confined by using lateral wires, such as depicted in Fig. 8. The images and their analysis with contour detection permit to evidence that in such a situation, the meniscus that is indeed pinned at the level of the wire induces the growth of the deposit through a complex flow pattern, essentially directed toward the corners. We actually do not monitor the flow pattern but deduce it from the contour detection of the deposit growth (Fig. 8, bottom). Again, this is an illustration of the capillary nature of the induced growth, very similar to the capillary flow of a sessile drop but somehow seen from the side (and of course with a different symmetry). Once the crust front has grown on a length scale comparable to the width between the spacers, the front becomes flat and grows further without any memory of the initially two-dimensional flow pattern. Such an experiment illustrates well how the flow may develop due to the pinning of the contact line [see also the schematic illustration of Fig. 6(a)] and must be governed by capillary effects. The latter are by nature slaved to the removal rate of solvent which may explain the observed scaling $v_c \sim J_0$, the evaporation rate.

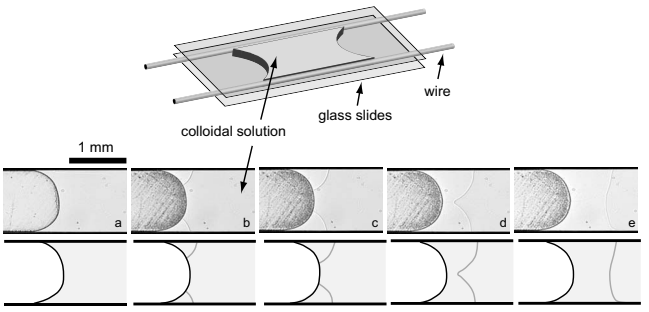

FIG. 8. A simple experiment to visualize how the crust builds up at the level of the meniscus: a drop of a colloidal solution is squeezed in between two microscope glass slides and confined by two wires (copper wire of 50 μm diameter) which also serve as spacers. Evaporation is directional (outward the cell), the meniscus is pinned, and optical micrographs clearly show the accumulation of a dense zone at the level of the meniscus. Contour detection and image reconstruction show that the "crust" has reached a steady shape with a boundary perpendicular to the wires—its propagation direction—after a of length scale roughly equal to the spacing between the wires (small colloids, ϕ=0.44, times of snapshots: (a) 0, (b) 72 min, (c) 125 min, (d) 325 min, (e) 374 min.)

[1] R. D. Deegan, O. Bakajin, T. F. Dupont, G. Huber, S. R. Nagel, and T. A. Witten, Nature (London) **389**, 827 (1997).
[2] R. D. Deegan, O. Bakajin, T. F. Dupont, G. Huber, S. R. Nagel, and T. A. Witten, Phys. Rev. E **62**, 756 (2000).
[3] R. D. Deegan, Phys. Rev. E **61**, 475 (2000).
[4] H. Hu and R. G. Larson, Langmuir **21**, 3972 (2005).
[5] H. Hu and R. G. Larson, Langmuir **21**, 3963 (2005).
[6] H. Hu and R. G. Larson, J. Phys. Chem. B **110**, 7090 (2006).
[7] W. D. Ristenpart, P. G. Kim, C. Domingues, J. Wan, and H. A. Stone, Phys. Rev. Lett. **99**, 234502 (2007).
[8] Y. O. Popov, Phys. Rev. E **71**, 036313 (2005).
[9] G. Berteloot, C.-T. Pham, A. Daerr, F. Lequeux, and L. Limat, EPL **83**, 14003 (2008).
[10] G. J. Dunn, S. K. Wilson, B. R. Duffy, S. David, and K. Sefi-

ane, Colloids Surf., A **323**, 50 (2008).
[11] K. S. Lee, C. Y. Cheah, R. J. Copleston, V. M. Starov, and K. Sefiane, Colloids Surf., A **323**, 63 (2008).
[12] T. A. Witten, EPL **86**, 64002 (2009).
[13] R. Zheng, Eur. Phys. J. E **29**, 205 (2009).
[14] D. J. Harris, H. Hu, J. C. Conrad, and J. A. Lewis, Phys. Rev. Lett. **98**, 148301 (2007).
[15] D. J. Harris and J. A. Lewis, Langmuir **24**, 3681 (2008).
[16] Y. Cai and B. Z. Newby, J. Am. Chem. Soc. **130**, 6076 (2008).
[17] I. U. Vakarelski, D. Y. C. Chan, T. Nonoguchi, H. Shinto, and K. Higashitani, Phys. Rev. Lett. **102**, 058303 (2009).
[18] W. M. Gelbart, R. P. Sear, J. R. Heath, and S. Chaney, Faraday Discuss. **112**, 299 (1999).
[19] E. Rabani, D. R. Reichman, P. L. Geissler, and L. E. Brus, Nature (London) **426**, 271 (2003).
[20] L. Pauchard and Y. Couder, EPL **66**, 667 (2004).
[21] N. Tsapis, E. R. Dufresne, S. S. Sinha, C. S. Riera, J. W. Hutchinson, L. Mahadevan, and D. A. Weitz, Phys. Rev. Lett. **94**, 018302 (2005).
[22] G. Marty and N. Tsapis, Eur. Phys. J. E **27**, 213 (2008).
[23] L. Xu, S. Davies, A. B. Schofield, and D. A. Weitz, Phys. Rev. Lett. **101**, 094502 (2008).
[24] T. Kajiya, D. Kaneko, and M. Doi, Langmuir **24**, 12369 (2008).
[25] D. S. Golovko, H. J. Butt, and E. Bonaccurso, Langmuir **25**, 75 (2009).
[26] L. Xu, A. Bergès, P. J. Lu, A. R. Studart, A. B. Schofield, H. Oki, S. Davies, and D. A. Weitz, Phys. Rev. Lett. **104**, 128303 (2010).
[27] F. Girard, M. Antoni, and K. Sefiane, Langmuir **26**, 4576 (2010).
[28] H. Bodiguel and J. Leng, Soft Matter (to be published).
[29] F. Clément and J. Leng, Langmuir **20**, 6538 (2004).
[30] P. N. Pusey and W. van Megen, Nature (London) **320**, 340 (1986).
[31] G. Brambilla, D. E. Masri, M. Pierno, L. Berthier, L. Cipelletti, S. Petekidis, and A. Schofield, Phys. Rev. Lett. **102**, 085703 (2009).
[32] A. Zosel, Colloid Polym. Sci. **271**, 680 (1993).
[33] Note that for small colloids, we report only the analysis for an initial volume fraction above a certain limit ($\phi_i \gtrsim 0.2$) for which the drop follows a typical course of events such as those depicted in Fig. 2. For a lower volume fractions, another scenario takes place for which the drop splits at some stage into two sub drops being still confined and touch the top and bottom plates.
[34] See supplementary material at http://link.aps.org/supplemental/10.1103/PhysRevE.82.021405 for movie of a droplet of a colloidal suspension.
[35] Although quite obvious from the evolution of $P(t)$, the onset of the shape instability can be assessed using for instance a shape parameter such as $[P(t)/2\pi]^2/A(t)$. When this parameter shows an upturn, it is a sign of an excess of perimeter as compared to the case of a circular drop and we can thus unambiguously define an instability time; we did not focus here on such a characterization but it is the core of a similar work published recently [45].
[36] B. J. Ackerson, S. E. Paulin, B. Johnson, W. van Megen, and S. Underwood, Phys. Rev. E **59**, 6903 (1999).
[37] It is however not clear why a crystal with a cell size comparable to the wavelength of light should depolarize light, but it does so indeed [Fig. 4(b)]. It is well known that the settling crystals are not equilibrium structures (with an isotropic face-centered cubic symmetry) but rather consists of faulty compact structures (e.g., random close-packed) for which the cubic isotropic structure disappears, and then becomes capable of depolarizing light. Yet, the use of ideas based on a continuous theory for objects with a size comparable to the wavelength of light remains dubious.
[38] A. S. Dimitrov and K. Nagayama, Langmuir **12**, 1303 (1996).
[39] K. Chen, S. V. Stoianov, J. Bangerter, and H. D. Robinson, J. Colloid Interface Sci. **344**, 315 (2010).
[40] More precisely, the drying Eq. (1) is rewritten to lead to a typical velocity for the recession of the meniscus $v_m = \dot{R}_m = d[(A/\pi)^{1/2}]/dt = (R_s/4\tau_e)/(x_m \ln x_m)$ with $x_m = R_m/R_s$. The latter function diverges around $x_m = 1$ which we do not explore; on the contrary, our conditions are $0.05 \lesssim x_m \lesssim 0.2$ in which case $-2R_s/\tau_e \lesssim v_m \lesssim -R_s/\tau_e$.
[41] J.-B. Salmon, private communication.
[42] E. R. Dufresne, E. I. Corwin, N. A. Greenblatt, J. Ashmore, D. Y. Wang, A. D. Dinsmore, J. X. Cheng, X. S. Xie, J. W. Hutchinson, and D. A. Weitz, Phys. Rev. Lett. **91**, 224501 (2003).
[43] L. Goehring, W. J. Clegg, and A. F. Routh, Langmuir **26**. 9269 (2010).
[44] L. Pauchard and C. Allain, EPL **62**, 897 (2003).
[45] L. Pauchard, M. Mermet-Guyennet, and F. Giorgiutti-Dauphiné, *Proceedings of the 8th European Coating Symposium* (Karisruhe, Germany, 2009), pp. 137–140.
[46] W. Schabel, I. Ludwig, and M. Kind, Drying Technol. **22**, 285 (2004).